Journal of Hazardous Materials 390 (2020) 122126

Contents lists available at ScienceDirect

Journal of Hazardous Materials

journal homepage: www.elsevier.com/locate/jhazmat

In-situ sulfuration of Cu-based metal-organic framework for rapid near-infrared light sterilization

Pengli Yu[a], Yajing Han[a,*], Donglin Han[a], Xiangmei Liu[b,*], Yanqin Liang[a], Zhaoyang Li[a], Shengli Zhu[a], Shuilin Wu[a,*]

[a] School of Materials Science & Engineering, the Key Laboratory of Advanced Ceramics and Machining Technology by the Ministry of Education of China, Tianjin University, Tianjin 300072, China

[b] Hubei Key Laboratory of Polymer Materials, Ministry-of-Education Key Laboratory for the Green Preparation and Application of Functional Materials, School of Materials Science & Engineering, Hubei University, Wuhan 430062, China

GRAPHICAL ABSTRACT

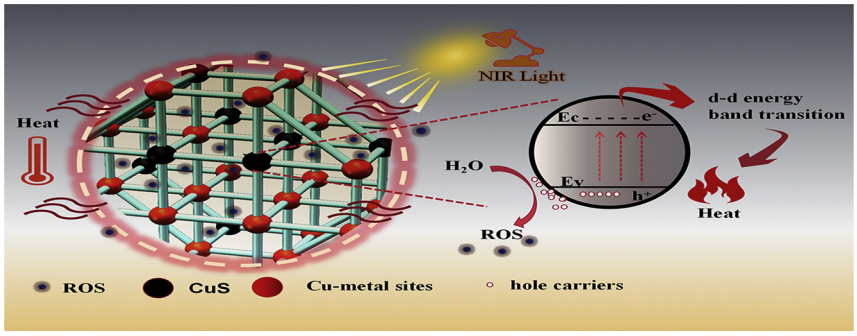

ARTICLE INFO

Editor: R. Teresa

Keywords:
Metal-organic framework
CuS
Photothermal
Photocatalysis
Antibacterial

ABSTRACT

Some new kinds of antibiotics-free antibacterial agents are required to deal with bacterial infections due to the occurrence of drug-resistance. In this work, Cu-based metal-organic framework (HKUST-1) embedded with CuS NPs were fabricated *via* a simple *in-situ* sulfuration process. The synthesized MOFs exhibited an highly effective disinfection efficacy of 99.70 % and 99.80 % against *Staphylococcus aureus* and *Escherichia coli* within 20 min irradiation of near-infrared (NIR) light, respectively, which was ascribed to the cooperative effects of photodynamic and photothermal effects of the composites. A certain amount of Cu^{2+} ions of the MOFs were reacted to form CuS NPs, which endowed this composite with outstanding photocatalytic and photothermal performance during NIR light irradiation. Moreover, HKUST-1 that composed of low toxic organic ligand 1,3,5-benzenetricarboxylic acid (H_3BTC) coordinating copper ions could be a controllable carrier that imposed certain constraint on the NPs. Hence, these CuS@HKUST-1 would be a promising bioplatform for rapid bacteria-killing.

1. Introduction

Some dangerous bacteria such as *Staphylococcus aureus* (*S. aureus*, Gram-positive bacteria) and *Escherichia coli* (*E. coli*, Gram-negative bacteria) are threatening human health (Fan et al., 2014), because once people drink the water polluted by these bacteria or the wounds are exposed to the environment with these bacteria, the bacterial infection and the followed complications will induce fatal diseases and even lead

* Corresponding authors.
E-mail addresses: hanyajing@tju.edu.cn (Y. Han), liuxiangmei1978@163.com (X. Liu), shuilinwu@tju.edu.cn, sxwsl1976@163.com (S. Wu).

https://doi.org/10.1016/j.jhazmat.2020.122126
Received 23 December 2019; Received in revised form 14 January 2020; Accepted 16 January 2020
Available online 17 January 2020

to death (Ferri et al., 2017). Currently, antibiotics are often clinically used for the therapy of bacterial infections (Raaymakers et al., 2017; Cullen et al., 2015). However, it is easy to arise antibiotic resistance and induce the occurrence of superbugs (Dhand et al., 2017; Macvane, 2017). Nowadays, new therapeutic strategies are needed urgently to treat recurrent bacterial infections, realizing rapid bacteria-killing with improbable resistance generation and low systemic toxicity to environment (Qi et al., 2017).

Recently, with the rapid development of photo-responsive materials, light has been emerged as an intriguing trigger for sterilization functions (Lismont et al., 2017). For example, photodynamic anti-bacterial (PDA) therapy has appeared as an alternative treatment to conventional antibiotics, which is effective in killing bacteria by generating reactive oxygen species (ROS) (Zhu et al., 2020). Moreover, short period of hyperthermia caused by photo-thermal effect can also destroy bacterial membrane and affect the protein structure, thus inactivating bacteria, which is called photothermal anti-bacterial (PTA) (Li et al., 2018a, b). So, combining these two kinds of methods, biomaterials with excellent photocatalytic and photothermal properties can be expected to efficiently kill bacteria with a nonresistant and minimally invasive process (Li et al., 2019; Jin et al., 2019). In recent years, increasing attention is drawn to the advanced materials such as ZnO, CuS, Bi_2O_3, Fe_2O_3, and TiO_2 that have been explored for photocatalytic inactivation of bacteria (Ahmed and Anbazhagan, 2017). Among the various photo-responsive materials, near-infrared (NIR)-responsive materials are more appropriate for antibacterial agents. NIR has little adverse effects on human beings and good penetrability (Chen et al., 2018; Xu et al., 2019). Copper sulfide nanoparticles (CuS NPs) are promising NIR-responsive materials with attractive properties such as good biocompatibility and low cost (Wang et al., 2015). The most important is that CuS NPs also can be used as PDA and PTA simultaneously (Hou et al., 2017). In addition, trace amount of copper ions can stimulate angiogenesis and collagen deposition, thus leading to a function of improving wound healing (Kornblatt et al., 2016; Sen et al., 2002).Wang *etc.* have reported a antibacterial application of cupric sulphide nanocomposite which displayed a high efficiency to degrade methylene blue (MB) under visible light and antibacterial property to *Bacillus subtilis* in 2018, and Gao *etc.* also have reported a novel antibacterial strategy utilizing the conjugation of Ce6 molecules and protein-modified CuS NPs under the irradiation in 2018 (Wang et al., 2018; Gao et al., 2018). Therefore, CuS NPs can be a quite appropriate antibacterial agent.

However, onefold CuS NPs usually present the aggregation tendency in solution, thus reducing their photo-catalytic efficiency (Lucky et al., 2015). For another, the excessive release of copper ions can lead to cytotoxicity and the direct contact with tissue may cause irritation, allergy and inflammation (Cao et al., 2012; Worthington et al., 2013). Therefore, in order to achieve a wider scope of antibacterial applications, it requires an effective carrier as a collaborative platform that imposing certain constraint on the CuS NPs. Constructing of metal ions and organic ligands, Metal-organic frameworks (MOFs) is a new type of composite materials which can be used as a carrier for NPs. (Lin et al., 2017). Among the many MOFs, HKUST-1, which is assembled by 1,3,5-benzenetricarboxylate (H_3BTC) coordinated copper ion, has been exhibiting enormous potential for practical applications, due to its regular porosity, excellent thermal stability, easy preparation and low cost (Lin and Hsieh, 2015). In addition, it is also compelling as an innovative dressing for treating chronic non-healing wounds (Xiao et al., 2018). Therefore, HKUST-1 can be a suitable carrier for CuS NPs. In addition, as a Cu-based MOF, the copper ion in itself can be used as copper source for the formation of CuS NPs, thus HKUST-1 may considerably simplify the preparation process and improve material utilization.

Herein, we reported a simple method to embed CuS NPs in MOF *via in-situ* sulfuration of HKUST-1, converting small amount of Cu^{2+} ions into CuS NPs, which was schematically illustrated in Scheme 1. Incorporating the merits of traditional photo-responsive agent of CuS NPs and flexible carrier HKUST-1, CuS@HKUST-1 can be an effective novel agent for rapid NIR-responsive antibacterial therapy. In this composite, CuS played a role in generating ROS and hyperthermia under the NIR light. The HKUST-1 can bind the position of the CuS NPs, preventing it from aggregating and contacting directly with tissue within the irradiation time. Therefore, HKUST-1 provided a framework for CuS NPs to work extremely efficiently, allowing ROS to spread freely in or out of the framework, and absorbing NIR light to produce heat, thereby achieving the purpose for rapid sterilization in a short time and improving biocompatibility in this process.

2. Experimental procedure

2.1. Synthesis of HKUST-1

HKUST-1 were synthesized by the method previously reported (Liu et al., 2010). 7.74 mmol $Cu(NO3)_2{\cdot}3H_2O$ and 4.28 mmol BTC (BTC = 1,3,5-benzenetricarboxylate) were dissolved in the 1:1:1 mixture (45 mL) of deionized water, ethanol, and dimethylformamide (DMF). The solution was heated to 75 °C and kept for 7 h in an oven. The resulting solution was cooled to ambient temperature. The MOF of HKUST-1 was obtained by centrifugation, then the precipitate was washed three times by ethanol, and dried under vacuum at room temperature.

2.2. Synthesis of CuS@HKUST-1

As synthesized HKUST-1 crystals (0.40 g) were immersed in the anhydrous ethanol (40 mL) solution of thioacetamide (0.6 g, 8 mmol) at 30 °C for various duration (S-3 : 3 h, S-4 : 4 h and S-5:5 h). After reaction, sample was filtered, and washed three times by ethanol, immersed sample in ethanol (100 mL) for 4 h before each cleaning, to remove the unreacted thioacetamide and its byproduct, which might remain in the pores of the MOF

2.3. Characterization

The surface morphology of samples was examined through scanning electron microscope (SEM, HITACHI S-4800, Tokyo, Japan) and elemental compositions of the CuS@HKUST-1 were determined on its fitted out with energy-dispersive X-ray spectrometry (EDS, X-MAX20). The Fourier-transformed infrared spectra (FTIR) was determined by a Thermo-scientific iS10 FT-IR spectrometer. The phase structure was examined through X-ray diffraction (XRD, Bruker D8 Advance). The UV–vis spectrophotometer (UV-2700, Shimadzu) was used to examine UV–vis diffuse reflectance absorption spectra (DRS). In the experiment, the photothermal and photodynamic performances were explored through a near-infrared light source (LOS-BLD-0808-005W-C).

2.4. Photothermal effects

These samples (HKUST-1, S-3, S-4 and S-5) as shown in Table S1, dispersed in the phosphate-buffered saline (500 μg/mL). Then the solutions were irradiated with NIR light source (808 nm, 0.8 W/cm^{-2}) for 20 min. And the temperature was recorded every minute intervals by using the Thermal Imager (FLIR-E50).

2.5. ROS detection and photocurrent test

Dichlorofluorescein diacetate (DCFH-DA) as a ROS sensor (Xie et al., 2017), was used to observed vitro ROS engender. In brief, the samples (HKUST-1, S-3, S-4 and S-5) dissolved in the DCFH dye solution were subjected to light (0.8 W/cm^{-2}) for 10 min, and recorded the fluorescence change in the solution every 1 min. Furthermore, the photocurrent of samples was also investigated by an electrochemical workstation (CHI 660E). In a three-electrode test system, using Na_2SO_4 (0.5 M) solution as the electrolyte, the photocurrent-time curves were

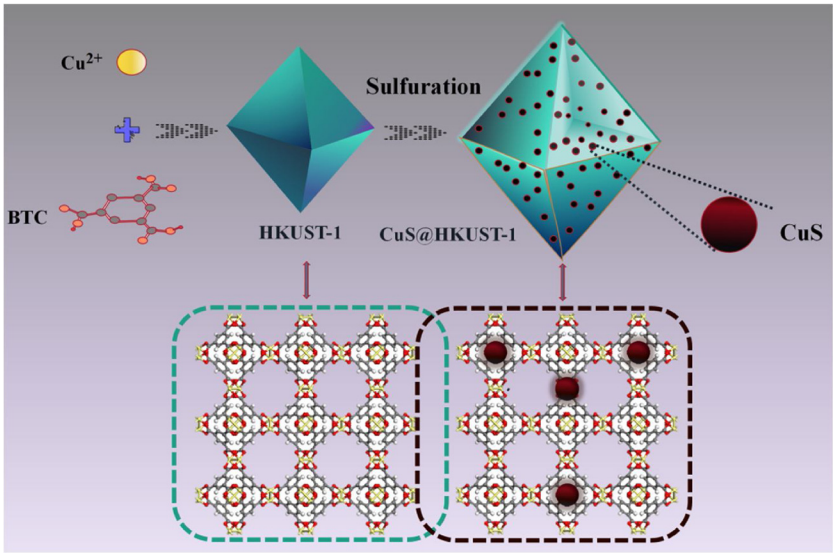

Scheme 1. Schematic illustration of the synthesis of the MOF.

tested by amperometric i-t mode with a potentiostat.

2.6. Cu^{2+} release in vitro

The release concentration of copper ions from CuS@H-HKUST-1 in 10 % phosphate buffer saline (PBS, pH 7.4, 37 °C) was obtained through Inductively-coupled plasma atomic emission spectrometry (ICP-AES). Added CuS@H-HKUST-1 solution (4 ml) into dialysis bag, then incubated in PBS (200 ml) with continuously stirred (100 rpm, 37 °C). Then at preseted intervals, replaced 4 mL release liquid with equal fresh PBS. Determined the amount of the copper by ICP-AES. Furthermore, the light effect on ion release were studied in 20 min.

2.7. In vitro antibacterial effects

S. aureus and *E. coli* were used to estimate the antibacterial performance of CuS@HKUST-1. The bacteria was cultured with sterilized liquid LB agar. In this study, different samples that containing pure PBS, HKUST-1, S-3, S-4 and S-5 (500 μg/mL) were mixed with about 10^7 CFU/mL^{-1} bacterial suspension. Then the 200 μL mixture was added into a 96 well plate for a cultivation of 20 min with or without NIR irradiation. After taking bacteria suspension for dilution, 20 μL bacterial solution was dispersed uniformly on LB agar plates before incubated for 24 h with 37 °C. Then taking photos of different agar plates for counting the colony units. The antibacterial efficiency of each plate was calculated *via* following equation (Mao et al., 2017; Zhang et al., 2018; Mao et al., 2018; Jin et al., 2018; Liu et al., 2013).

$$\text{Antibacterial ratio}(\%) = (1 - \frac{\text{CFUexperimental group}}{\text{CFUcontrol group}}) \times 100\%$$

2.8. Bacterial morphological studies

After the antibacterial experiments, the bacterial morphologies co-cultured with the samples were examined by SEM. The previous treatment was consistent with the antibacterial experiment except that a sheet glass was added to each 96 well plate. After an incubation period of 20 min with or without NIR irradiation, the sheet glass was taken from the 96-well plate after 1 h of standing precipitation, and mixed with glutaraldehyde solution (2.5 %) for 2 h, then dehydrated in gradient ethanol (30, 50, 70, 80, 90 and 100 %) for 15 min sequentially. After drying, the bacterial morphologies were investigated by SEM.

2.9. Cytotoxicity studies

NIH-3T3 cells were used to implement the MTT assay for *in vitro* cytotoxicity evaluation. Firstly, the cells (2.5×10^4 per mL) were incubated in 96-well plates for 1 day and 3 days. After removing the supernatant, 90 μl of fresh medium and 10 μl MTT reagent were added and cultured for 4 h. After removing the medium, 110 μL Formazan solution was added and specimens' optical absorption at 490 nm was recorded. The cell viability of different samples was valued by comparing the values with the control. Simultaneously, the samples under NIR irradiation was also considered. Before incubation, the cells that seeded onto the 96-well plates received 20 min NIR light irradiation.

3. Results and discussion

3.1. Characterization of CuS@HKUST-1

The as-synthesized HKUST-1 MOF exhibited morphologically octahedral structure with distinct edges in Fig. S1a. After sulfuration, the morphologies of MOFs were shown in Fig. 1. Regardless of sulfuration time, three kinds of MOFs exhibited an octahedral shape with an average size of 3 μm. When the reaction was performed at 30 °C for 3 h, the surface had a chiseled and geometrical shape which was consistent with pristine MOFs (Fig. 1a). But when the reaction times increasing such as 5 h (Fig. 1c), the surface became increasingly rougher and the octahedral shape changing into slightly distorted and collapsed. Furthermore, when the reaction times extended to 12 h, the shape of HKUST-1 completely disappeared, as seen in Fig. S1b, only agglomerated massive particles was left. In addition, EDX elemental maps showed that Cu and S were evenly spread in the samples (Fig. 1d). These results suggested the successful sulfuration of Cu-MOF. With the extension of sulfurization time, the amount of nano-CuS increased in HKUST-1 from about 1.8 wt% to 2.0 wt%, and then 2.3 wt% (Table S1).

Fig. 2a showed the XRD patterns of the pristine HKUST-1 and sulfurized MOFs. The HKUST-1 displayed a strongest peak at 10.6°. As the sulfuration time increased, the diffraction intensities decreased and diffraction peaks broadened, which indicated that the crystallinity declined and the MOF host structure might be destroyed (Moon et al., 2013). Furthermore, when the reaction last as long as 12 h, the samples appeared only the peaks that belong to CuS as shown in the inset of Fig. 2a, suggesting that almost all HKUST-1 was changed into CuS (Du et al., 2007).

FT-IR were recorded to display the coordination in MOF as shown in

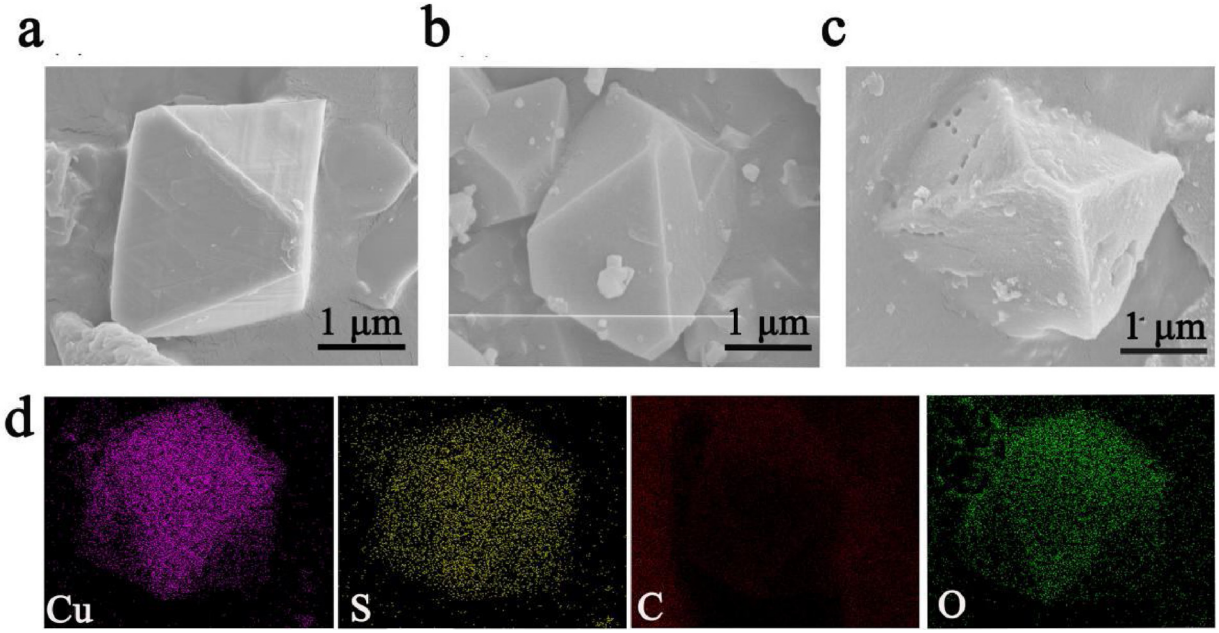

Fig. 1. Characterization of the synthesized MOF, SEM images of S-3 (a), S-4 (b) and S-5 (c). (d) EDS elemental mapping of Cu, S, C, and O elements of S-4.

Fig. 2b. The peaks at 1450 and 1649 cm^{-1}, indicated −O−C−O− bond. In addition, the peaks at 1373 and 1548 cm^{-1} indicated the stretching of C═C, and the peaks at 729 cm^{-1} and 490 cm^{-1} represented the bonding of benzene-ring and Cu−O, respectively (Xiao et al., 2017; Azhar et al., 2016). Moreover, the band related to the bonding between Cu−O disappeared when sulfuration for 12 h, as a result of the sulfuration of all copper ions in the HKUST-1.

3.2. NIR photothermal performance

The light absorption intensity of different samples were evaluated by the UV–vis spectrophotometer in Fig. 3. It could be observed that when the sulfuration time was increased, the absorption around the NIR region of MOFs was continuously improved, which was attributed to the increased amount of CuS NPs. These results illustrated that long time sulfuration was beneficial for the formation of more CuS NPs, thus enhancing the NIR absorption ability of sulfurized MOFs.

To investigate the photothermal properties of the samples, HKUST-1, S-3, S-4, and S-5 were irradiated in PBS by NIR light (808 nm, 0.8 W/cm^{-2}). As shown in Fig. 4b, the temperatures of pure PBS solution rose

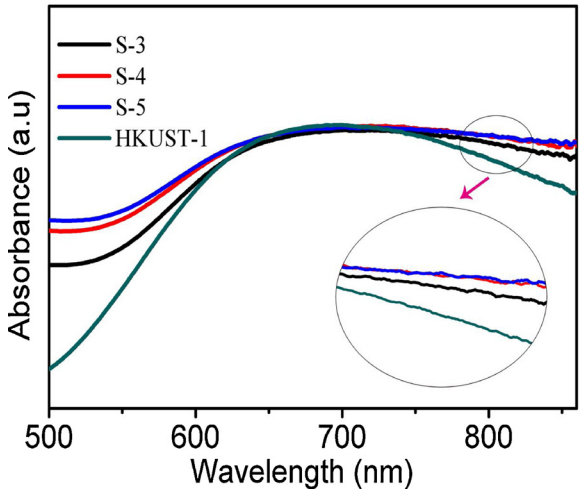

Fig. 3. UV–vis absorption spectrum of HKUST-1, S-3, S-4, S-5.

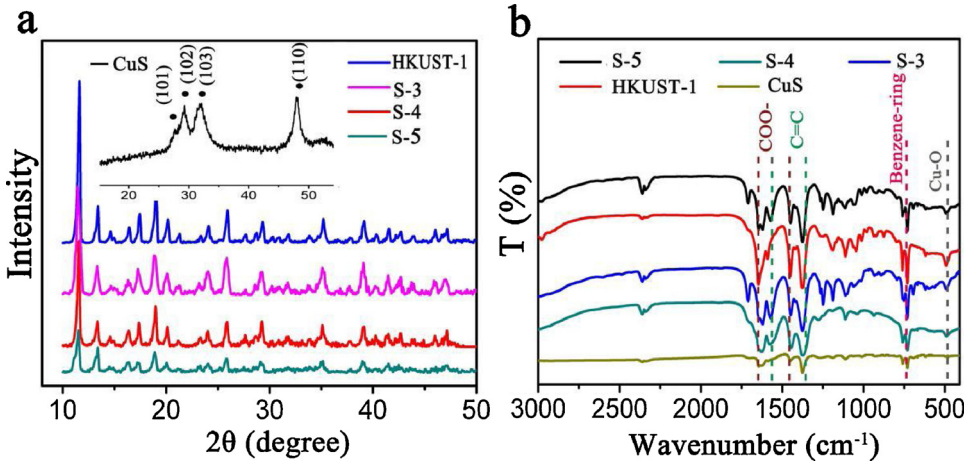

Fig. 2. (a) XRD patterns of HKUST-1, S-3, S-4, S-5. Inset: PXRD pattern of CuS converted by HKUST-1. (b) FT-IR spectra of HKUST-1, S-3, S-4, S-5 and CuS converted by HKUST-1.

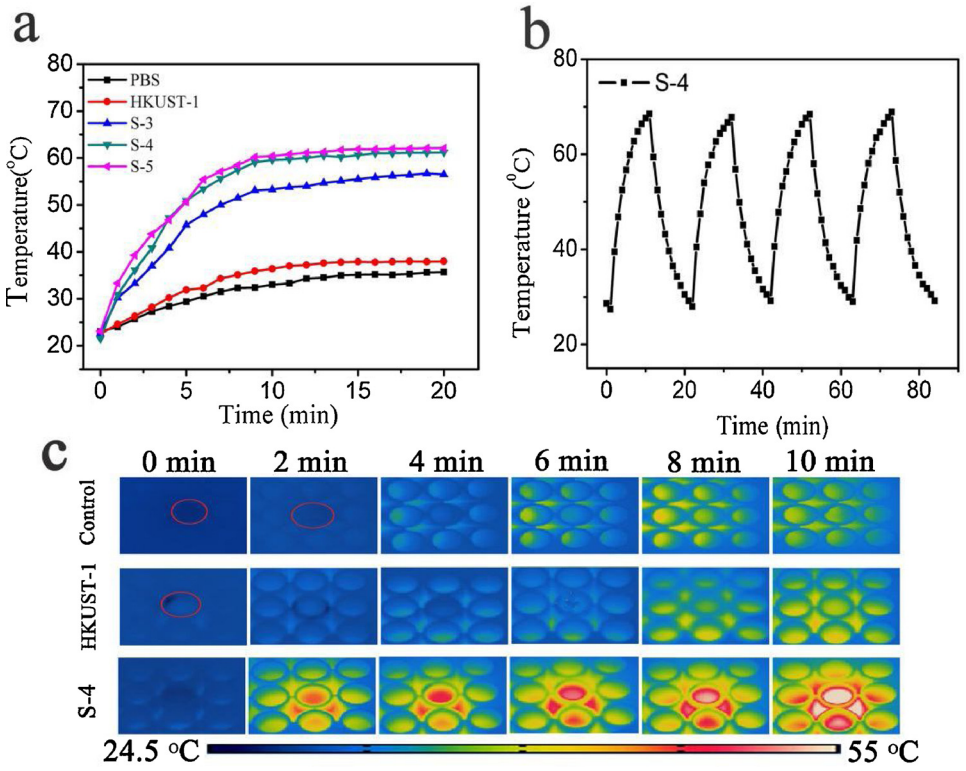

Fig. 4. (a) The photothermal curves of HKUST-1, S-3, S-4, S-5 under the irradiation of 808 nm light. (b) Transient thermal measurements of S-4 under repeated laser on-off cycles of NIR light irradiation. (c) Real-time infrared thermal images of exemplary samples (S-4) dissolved into PBS aqueous solution.

slowly and reached a low plateau after irradiation for 12 min. Similarly, the pristine HKUST-1 exhibited no obvious photothermal property, which temperature only increased from 23 to 35 °C under light for 20 min. By contrast, the temperature increased quickly after sulfurization treatment with the pristine MOFs. These samples rapidly rose to a relatively high temperature and reached a plateau after 10 min of NIR light irradiation. The maximal temperature of sample S-3, S-4, and S-5 is 56.8, 60.7 and 62.5 °C, respectively. Apparently, more sulfuration time for HKUST-1 led to a higher photothermal temperature caused by more CuS NPs generated in the MOFs, which played an important role in the absorption of NIR light. Considering the higher temperature can induce adverse effects to normal tissues while lower temperature has lower antibacterial effects, the sample of S-4 was selected for further study. Furthermore, as shown in Fig. 4b, the laser on-off cycles of S-4 exhibited that the temperature of this samples had a good photostability even at a higher temperature caused by stronger irradiation (1 W/cm^{-2}). In addition, Fig. 4c showed representative real-time infrared thermal images of typical samples under continuous NIR irradiation for 10 min. Clearly, the temperature of control group and HKUST-1 showed minimal changes, which was in line with previous studies. As a contrast, CuS@HKUST-1 showed obvious temperature variation.

3.3. NIR photocatalysis

To evaluate the photocatalytic effects of the CuS@HKUST-1, the photo-induced ROS was detected using DCFH-DA (Xiang et al., 2019). As displayed in Fig. 5a, almost all samples exhibited no fluorescence intensity (FL) signal in the dark, indicating little catalytic ability of these samples. There was almost no fluorescence intensity (FL) signal detected in control group (PBS under 808 nm NIR irradiation) in Fig. 5b. Meanwhile, HKUST-1 showed negligible change, indicating no ROS. In contrast, the FL signal showed distinct enhancement when the ROS probe contacted with the CuS@HKUST-1 under the irradiation of 808 nm NIR. After irradiation under NIR light for 10 min, S-3, S-4 and S-5 showed 26, 23 and 15.5 fold enhancement of FI compared to the control group, respectively. It could be found that both S-3 and S-4 have a higher enhancement of FL than S-5, which may be caused by the structure destroying of HKUST-1 and some aggregation of CuS particles. In addition, S-3 even showed a slight enhancement of FL than S-4, possibly due to the more optimum dispersion states of CuS nanoparticles as well as the more integrated and appropriate hierarchical structure in the sample S-3. This may be able to benefit free carriers to migrate to the nanoparticles surface and react to produce ROS (Li et al., 2014; Wen et al., 2017; Ramasubbu et al., 2017). Furthermore, the integrity of the MOF structure may be conducive to ROS transmission (Falcaro et al., 2016). At the same time, the photocurrent response of these samples was also investigated in Fig. 5c. Both S-3 and S-4 could generate more number of electrons under NIR light, suggesting the faster rate of separating holes and electrons, followed by S-5 and HKUST-1. This was similar to the previous ROS detection.

As a p-type semiconductor, CuS NPs have a clearly localized surface plasmon resonance (LSPR) within NIR region (Liu et al., 2015). Under NIR light, the intrinsic d-d transition of Cu^{2+} can be triggered, which could result in photothermal performance (Chen et al., 2019). On the other side, CuS NPs as a self-doped materials, have a high-concentration free carries (hole carriers) on the basis of intrinsic copper deficiency in their lattice (Liu and Swihart, 2014; Comin and Manna, 2014). CuS particles embedded in the framework maintained a strong NIR absorbance performance and these hole carriers in CuS NPs could probably react with H_2O to produce ROS ($^{\cdot}OH$) (Li et al., 2018a, b; Chang et al., 2018). HKUST-1 can be a suitable carrier that serves as a conducive place for these reaction processes. These results illustrate that the composites have a great potential as a photothermal and photodynamic agent for biological applications by fabricating CuS nanoparticles in HKUST-1, as shown in Fig. 6.

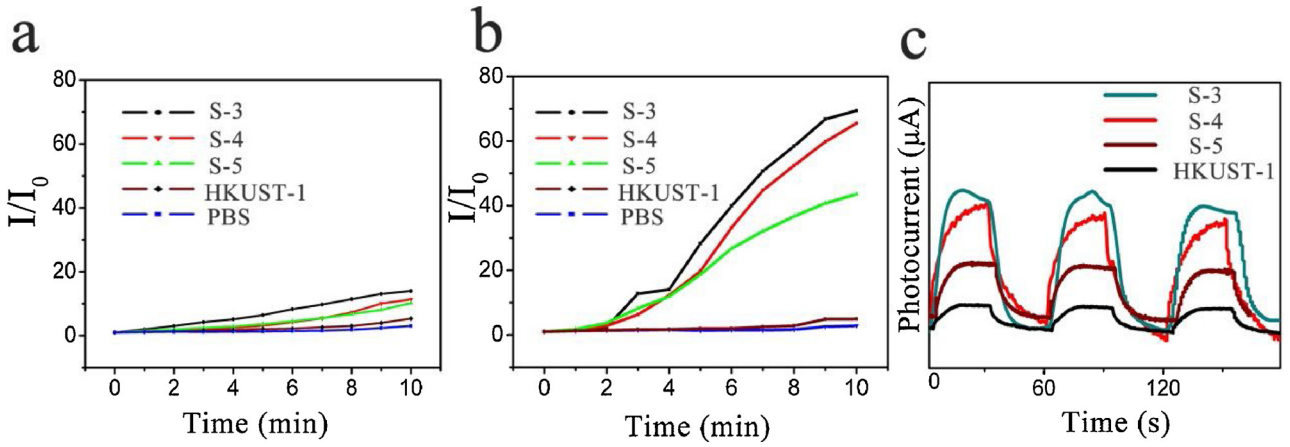

Fig. 5. (a) Fluorescence intensity (FI) of DCF at 525 nm with different samples immersed in the fluorescent dye solution without NIR light. I_0 : FI in initial value, I: FI in different time. (b) FI of different samples under light conditions. (c) Photocurrent responses of samples.

3.4. Copper ion release behaviors

The release behaviors of CuS@HKUST-1 were studied in 10 % PBS at 37 °C. As shown in Fig. 7a, for all the samples, after 12 h, the release rate of copper ions increased dramatically, which may be due to the instability of HKUST-1 in PBS (Decoste et al., 2012). By comparison, as the sulfuration time increased, the samples had a slightly faster release rate, which was possibly ascribed to the fact that the increase of CuS amount in MOFs further exacerbated the instability of HKUST-1 in PBS after 12 h. Additionally, the effect of NIR light on the copper ion release rate within 20 min was investigated in Fig. 7b. It was observed that for HKUST-1, whether there was light or not, the release of copper ions had no obvious change within a short time. However, for S-4, there was a significantly increase under the light. The potential reason may be that the CuS NPs embedded within HKUST-1 can absorb light more effectively and change it into heat compared to the HKUST-1, which may results in the uneven distribution of heat on the whole CuS@HKUST-1 (Wang et al., 2016), and the followed structural breakdown of partial MOFs, thus releasing more copper ions.

3.5. Antibacterial activity in vitro

The spread plate method was used to analyze the antibacterial efficacy of CuS@HKUST-1 against *E. coli* and *S. aureus*, which represented the major common species among most bacterial infections (Schnaider et al., 2017). As shown in Fig. 8a and b, the bacterial counts of the control group (PBS) were similar, whether or not there was light irradiation, suggesting no antibacterial activity. In comparison, when the samples were treated under 808 nm lasers for 20 min, both S-4 and S-5 showed considerable antibacterial effect, the number of bacterial CFUs in both of them had been plummeting, and the corresponding antibacterial efficacy rose up to 99.75 % and 99.72 % against *S. aureus* (Fig. 8c) and 99.85 % and 99.87 % against *E. coli* (Fig. 8d), respectively. Whereas, pristine HKUST-1 showed a small decrease in surviving bacteria under the same condition. It was similar to the control group that had no distinct effect. Furthermore, without light irradiation, the bacterial colonies on these groups (HKUST-1, S-3, S-4, and S-5) changed little, indicating no obvious antibacterial effect. The lesser antibacterial effect might be attributed to the small amount of Cu ions released in darkness. For further researching, the antibacterial effect after culturing with representative samples (control, HKSUT-1 and S-4) for 24 h in darkness was investigated, as shown in Fig. S2. After culturing for 24 h, the bacterial colonies were decreased by over 70 percent for *S. aureus* and *E. coli*. And S-4 showed a better antibacterial properties compared with HKUST-1 which may be due to the more Cu ions release.

The morphologies of bacteria that treated with representative

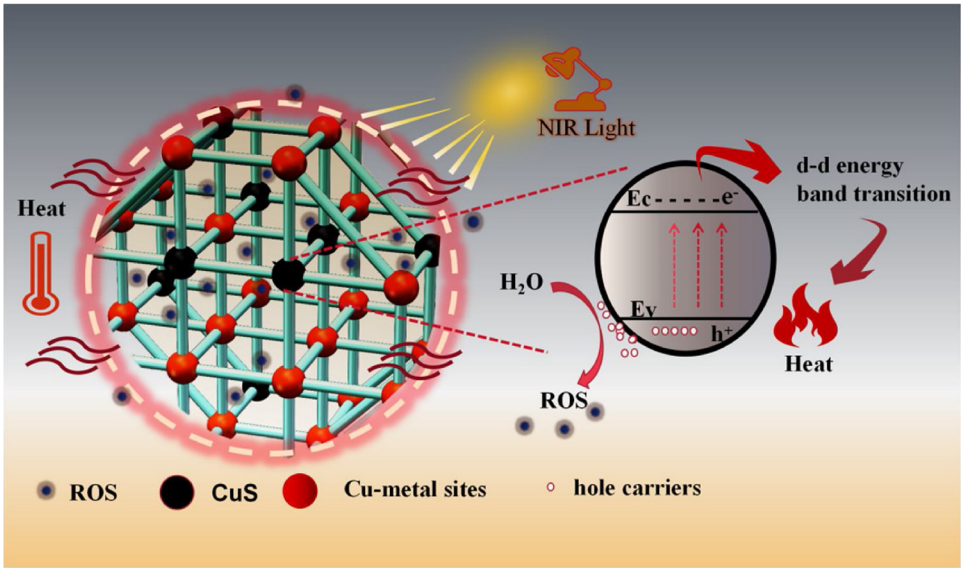

Fig. 6. Illustration of photothermal and photodynamic performance process in CuS@HKUST-1 under NIR light.

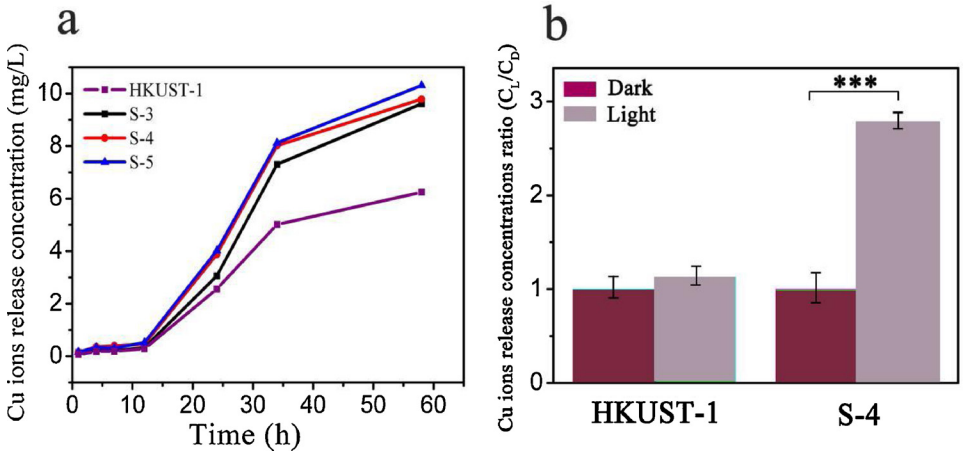

Fig. 7. (a) Cumulative amounts of Cu ions released from the HKUST-1, S-3, S-4 and S-5 in 10 % PBS at 37 °C. (b) The Cu ions release ratio under light, or not. C_D: cumulative amounts of Cu ions in dark within 20 min. C: cumulative amounts of Cu ions for samples within 20 min.

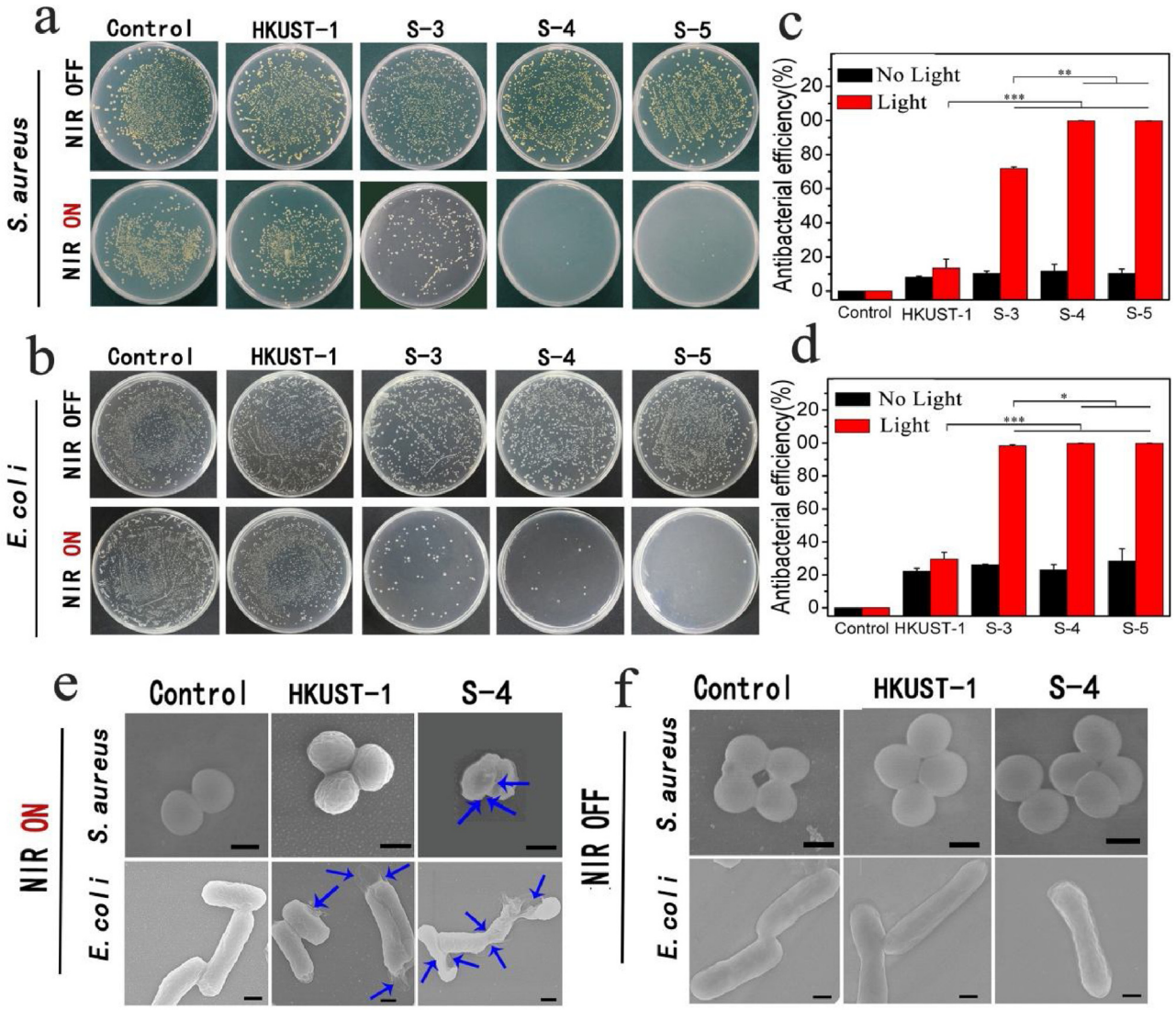

Fig. 8. The *in vitro* antibacterial activity against *S. aureus* (a) and *E. coli*. (b). The statistics results of the antibacterial ability of *S. aureus* (c), and *E. coli* (d), and error bars indicate means ± standard deviations: *P < 0.05, **P < 0.01, and ***P < 0.001. The morphologies and structures of *S. aureus* (e) and *E. coli* (f), with or without light for different samples. Scale bars are 400 nm.

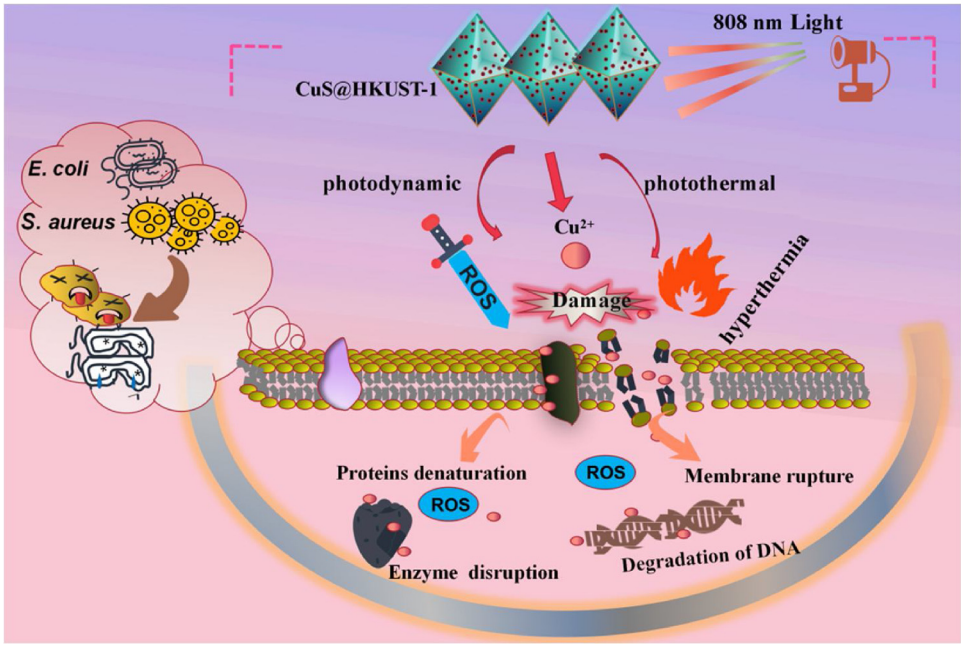

Fig. 9. Illustration of the synergistic behaviors in antibacterial processes with the CuS@HKUST-1 under 808 nm NIR light irradiation.

samples were examined by SEM. Fig. 8e and f illustrated that the bacteria in the control group retained a complete, compact and typical morphologies, indicating that the samples were nontoxic against bacteria. By contrast, there was a significant difference from the control group when the bacteria treated with CuS@HKUST-1 (S-4) under NIR light. The bacterial membranes had obvious distortion, which became shrunken and wrinkled or even cracks as marked by blue arrows. However, when there was no irradiation, bacteria mostly kept the original shape with integrated cell walls. These results were in good agreement with the spread plate results, only under NIR light irradiation, the as-prepared MOFs can exhibit highly effective antibacterial efficacy.

Fig. 9 showed the antibacterial mechanism based on the above results. Under the NIR irradiation, CuS@HKUST-1 can utilize effective NIR absorbance to convert light into heat. Hyperthermia can cause irreversible cellular membrane damage by loosening cell membranes and increasing membrane permeability (Sortino, 2012). Meanwhile, it could also result in the denaturation of proteins (Svaasand et al., 1990). Moreover, the ROS generated by CuS@HKUST-1 under light irradiation, can be more easier to oxidize DNA, certain enzymes or proteins (Xu et al., 2016), benefiting from membrane destruction caused by photoinduced hyperthermia. Over pre-existing antibacterial action, the Cu ions released from CuS@HKUST-1 could also more easily assist in killing bacteria by means of damaging the DNA structure, vital enzymes and proteins, as well as causing intracellular substance leakage (Wyszogrodzka et al., 2016; Burghardt et al., 2015). Based upon the interaction of all of these factors, CuS@HKUST-1 can show efficient antibacterial effects within 20 min NIR light irradiation.

3.6. Cytotoxicity

In order to investigate the affects of samples on mammalian cell growth, HKUST-1, S-3, S-4 and S-5 toward NIH-3T3 were evaluated through the MTT assay for day 1 and 3. As shown in Fig. 10a, without NIR light, all the samples had similar influences on the cells, exhibiting certain degree of inhibition to the growth of cell. The cells viability of all groups was around 60%–70%. By contrast, the degree of restriction of cell growth was increased in S-3, S-4 and S-5 when exposed to NIR irradiation. This could be caused by the ROS and hyperthermia produced from these samples (Han et al., 2020). Moreover, after three days of cultivation with changing the medium regularly, the cell viability had some promotion as can be seen in Fig. 10b. In consideration of the fact that HKUST-1 tended to be unstable in the cell culture medium, which could result in a relatively faster copper release after 24 h cultivation, these samples possessed certain degree of inhibition to the cell growth. However, in the experiments, there were still numerous cells that survived and grew after treatment. It revealed that the CuS@HKUST-1 exhibited the acceptable effects on the cell viability, demonstrating the feasibility of CuS@HKUST-1 for rapid sterilization under NIR irradiation.

4. Conclusion

In this work, CuS@HKUST-1 composites have been successfully fabricated *via* simple *in-situ* sulfuration process, in which the HKUST-1 acted as a tunable carrier platform for CuS NPs. In this way, the photoresponsive properties of CuS, under NIR irradiation was brought into full play. After 20 min of light irradiation, the composites exhibited excellent antibacterial effect of over 99.70 % and 99.80 % against *S. aureus* and *E. coli*, respectively, on account of the tripartite synergy of PTA, PDA and released Cu ions. Additionally, even if a long time in contact with the mammalian cell, CuS@HKUST-1 showed acceptable effect on cell growth. This study may provide a promising paradigm for biomedical applications of HKUST-1, achieving a rapid and effective sterilization for bacterial polluted environment.

CRediT authorship contribution statement

Pengli Yu: Conceptualization, Methodology, Data curation, Writing - original draft. **Yajing Han:** Conceptualization, Methodology, Data curation. **Donglin Han:** Methodology, Data curation, Writing - original draft, Project administration. **Xiangmei Liu:** Conceptualization, Writing - review & editing, Supervision, Project administration. **Yanqin Liang:** Methodology. **Zhaoyang Li:** Methodology. **Shengli Zhu:** Methodology. **Shuilin Wu:** Conceptualization, Writing - review & editing, Supervision, Project administration.

Declaration of Competing Interest

The authors declare that they do not have any financial relation

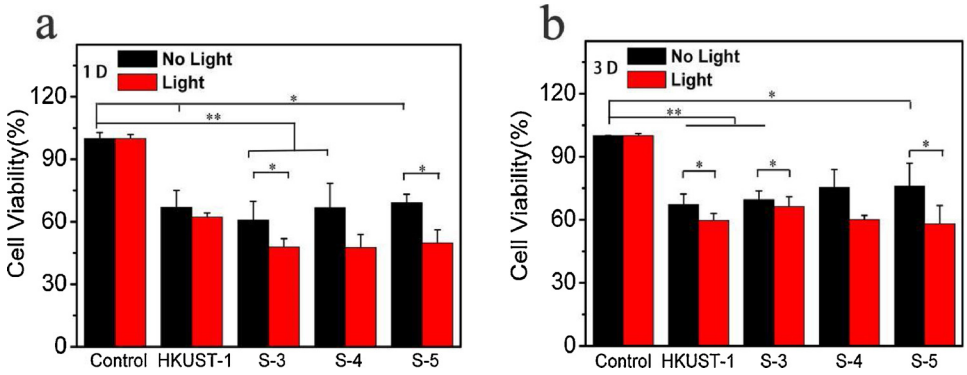

Fig. 10. MTT assay of cell viabilities cultured in the medium with different samples after co-culture for 1 day (a), 3 days (b). The error bar indicate means ± standard deviations (n = 3): *P < 0.05 and **P < 0.01.

with the commercial identities or associative interests that represents a conflict of interest in connection with the work submitted.

Acknowledgments

This work was jointly supported by the National Science Fund for Distinguished Young Scholars51925104, and the National Natural Science Foundation of China (Nos. 51671081, and 51871162) as well as the Natural Science Fund of Hubei Province (2018CFA064).

Appendix A. Supplementary data

Supplementary material related to this article can be found, in the online version, at doi:https://doi.org/10.1016/j.jhazmat.2020.122126.

References

Ahmed, K.B., Anbazhagan, V., 2017. Synthesis of copper sulfide nanoparticles and evaluation of *in vitro* antibacterial activity and *in vivo* therapeutic effect in bacteria-infected zebrafish. RSC Adv. 7 (58), 36644–36652.
Azhar, M.R., Abid, H.R., Sun, H., Periasamy, V., Tade, M.O., Wang, S., 2016. Excellent performance of copper based metal organic framework in adsorptive removal of toxic sulfonamide antibiotics from wastewater. J. Colloid Interface Sci. 478, 344–352.
Burghardt, I., Luthen, F., Prinz, C., Kreikemeyer, B., Zietz, C., Neumann, H., Rychly, J., 2015. A dual function of copper in designing regenerative implants. Biomaterials 44, 36–44.
Cao, B., Zheng, Y., Xi, T., Zhang, C., Song, W., Burugapalli, K., Yang, H., Ma, Y., 2012. Concentration-dependent cytotoxicity of copper ions on mouse fibroblastsin vitro: effects of copper ion release from TCu380A vs TCu220C intra-uterine devices. Biomed. Microdevices 14, 709–720.
Chang, Y., Cheng, Y., Feng, Y., Jian, H., Wang, L., Ma, X., Li, X., Zhang, H., 2018. Resonance energy transfer-promoted photothermal and photodynamic performance of gold-copper sulfide yolk-shell nanoparticles for chemophototherapy of cancer. Nano Lett. 18, 886–897.
Chen, Y., Li, W., Li, L., Wang, L., 2018. Progress in organic photocatalysts. Rare Met. 37, 1–12.
Chen, J., Ning, C., Zhou, Z., Yu, P., Zhu, Y., Tan, G., Mao, C., 2019. Nanomaterials as photothermal therapeutic agents. Prog. Mater. Sci. 99, 1–26.
Comin, A., Manna, L., 2014. New materials for tunable plasmonic colloidal nanocrystals. Chem. Soc. Rev. 43, 3957–3975.
Cullen, T.W., Schofield, W.B., Barry, N.A., Putnam, E.E., Rundell, E.A., Trent, M.S., Trent, M.S., Degnan, P.H., Booth, C.J., Goodman, A.L., 2015. Antimicrobial peptide resistance mediates resilience of prominent gut commensals during inflammation. Science 347, 170–175.
Decoste, J.B., Peterson, G.W., Smith, M.W., Stone, C.A., Willis, C.R., 2012. Enhanced stability of Cu-Btc MOF via perfluorohexane plasma-enhanced chemical vapor deposition. J. Am. Chem. Soc. 134, 1486–1489.
Dhand, C., Venkatesh, M., Barathi, V.A., Harini, S., Bairagi, S., Leng, E.G.T., Muruganandham, N., Low, K.Z.W., Fazil, M.H.U.T., Loh, X.J., Srinivasan, D.K., Liu, S., Beuerman, R.W., Verma, N.K., Ramakrishna, S., Lakshminarayanan, R., 2017. Bio-inspired crosslinking and matrix-drug interactions for advanced wound dressings with long-term antimicrobial activity. Biomaterials 138, 153–168.
Du, W., Qian, X., Ma, X., Gong, Q., Cao, H., Yin, J., 2007. Shape-controlled synthesis and self-assembly of hexagonal covellite (CuS) nanoplatelets. Chem. – Eur. J. 13 (11), 3241–3247.
Falcaro, P., Ricco, R., Yazdi, A., Imaz, I., Furukawa, S., Maspoch, D., Ameloot, R., Evans, J.D., Doonan, C.J., 2016. Application of metal and metal oxide nanoparticles@MOFs coord. Chem. Rev. 307, 237–254.
Fan, Z., Liu, B., Wang, J., Zhang, S., Lin, Q., Gong, P., Ma, L., Yang, S., 2014. A novel wound dressing based on Ag/graphene polymer hydrogel: effectively kill bacteria and accelerate wound healing. Adv. Funct. Mater. 24 39330–3943.
Ferri, M., Ranucci, E., Romagnoli, P., Giaccone, V., 2017. Antimicrobial resistance: a global emerging threat to public health systems. Crit. Rev. Food Sci. Nutr. 57, 2857–2876.
Gao, D., Ji, X., Wang, J., Wang, Y., Li, D., Liu, Y., Chang, K., Qu, J., Zheng, J., Yuan, Z., 2018. Engineering a protein-based nanoplatform as an antibacterial agent for light activated dual-modal photothermal and photodynamic therapy of infection in both the NIR I and II windows. J. Mater. Chem. B 6 (5), 732–739.
Han, D., Han, Y., Li, J., Liu, X., Yeung, K.W.K., Zheng, Y., Cui, Z., Yang, X., Liang, Y., Li, Z., Zhu, S., Yuan, X., Feng, X., Yang, Cao, Wu, S., 2020. Enhanced photocatalytic activity and photothermal effects of Cu-doped metal-organic frameworks for rapid treatment of bacteria-infected wounds. Appl. Catal. B 261, 118248.
Hou, L., Shan, X., Hao, L., Feng, Q., Zhang, Z., 2017. Copper sulfide nanoparticle-based localized drug delivery system as an effective cancer synergistic treatment and theranostic platform. Acta Biomater. 54, 307–320.
Jin, C., Su, K., Tan, L., Liu, X., Cui, Z., Yang, X., Li, Z., Liang, Y., Zhu, S., Yeung, K.W.K., Wu, S., 2019. Near-infrared light photocatalysis and photothermy of carbon quantum dots and au nanoparticles loaded titania nanotube array. Mater. Des. 177, 107845.
Jin, C., Liu, X., Tan, L., Cui, Z., Yang, X., Zheng, Y., Yeung, K.W.K., Chu, P.K., Wu, S., 2018. Ag/AgBr-loaded mesoporous silica for rapid sterilization and promotion of wound healing. Biomater. Sci. 6, 1735–1744.
Kornblatt, A.P., Nicoletti, V.G., Travaglia, A., 2016. The neglected role of copper ions in wound healing. J. Inorg. Biochem. 161, 1–8.
Li, B., Tan, L., Liu, X., Li, Z., Cui, Z., Liang, Y., Zhu, S., Yang, X., Yeung, K.W.K., Wu, S., 2019. Superimposed surface plasma resonance effect enhanced the near-infrared photocatalytic activity of Au@Bi_2WO_6 coating for rapid bacterial killing. J. Hazard. Mater. 380, 120818.
Li, R., Hu, J., Deng, M., Wang, H., Wang, X., Hu, Y., Jiang, H., Jiang, J., Zhang, Q., Xie, Y., Xiong, Y., 2014. Integration of an inorganic semiconductor with a metal–organic framework: a platform for enhanced gaseous photocatalytic reactions. Adv. Mater. 26, 4783–4788.
Li, Y., Liu, X., Tan, L., Cui, Z., Yang, X., Zheng, Y., Yeung, K.W.K., Chu, P.K., Wu, S., 2018a. Rapid sterilization and accelerated wound healing using Zn^{2+} and graphene oxide modified g-C_3N_4 under dual light irradiation. Adv. Funct. Mater. 28, 1800299.
Li, M., Liu, X., Tan, L., Cui, Z., Yang, X., Li, Z., Zheng, Y., Yeung, K.W.K., Chu, P.K., Wu, S., 2018b. Noninvasive rapid bacteria-killing and acceleration of wound healing through photothermal/photodynamic/copper ion synergistic action of a hybrid hydrogel. Biomater. Sci. 6, 2110–2121.
Lin, K.A., Hsieh, Y., 2015. Copper-based metal organic framework (MOF), HKUST-1, as an efficient adsorbent to remove p-nitrophenol from water. J. Taiwan Inst. Chem. Eng. 50, 223–228.
Lin, S., Liu, X., Tan, L., Cui, Z., Yang, X., Yeung, K.W.K., Pan, H., Wu, S., 2017. Porous iron-carboxylate metal–organic framework: a novel bioplatform with sustained antibacterial efficacy and nontoxicity. ACS Appl. Mater. Interfaces 9, 19248–19257.
Lismont, M., Dreesen, L., Wuttke, S., 2017. Metal-organic framework nanoparticles in photodynamic therapy: current status and perspectives. Adv. Funct. Mater. 27, 1606314.
Liu, X., Swihart, M.T., 2014. Heavily-doped colloidal semiconductor and metal oxide nanocrystals: an emerging new class of plasmonic nanomaterials. Chem. Soc. Rev. 43, 3908–3920.
Liu, J., Wang, Y., Benin, A.I., Jakubczak, P., Willis, R.R., Levan, M.D., 2010. CO_2/H_2O adsorption equilibrium and rates on metal – organic frameworks: HKUST-1 and Ni/DOBDC. Langmuir 26, 14301–14307.
Liu, X., Mou, Y., Wu, S., Man, H.C., 2013. Synthesis of silver-incorporated hydroxyapatite nanocomposites for antimicrobial implant coatings. Appl. Surf. Sci. 273, 748–757.
Liu, M., Xue, X., Ghosh, C., Liu, X., Liu, Y., Furlani, E.P., Swihart, M.T., Prasad, P.N., 2015. Room-temperature synthesis of covellite nanoplatelets with broadly tunable localized surface plasmon resonance. Chem. Mater. 27, 2584–2590.
Lucky, S.S., Soo, K.C., Zhang, Y., 2015. Nanoparticles in photodynamic therapy. Chem. Rev. 115, 1990–2042.
Macvane, S.H., 2017. Antimicrobial resistance in the intensive care unit - a focus on gram-negative bacterial infections. Eur. J. Intensive Care Med. 32 (1), 25–37.
Mao, C., Xiang, Y., Liu, X., Cui, Z., Yang, X., Yeung, K.W.K., Pan, H., Wang, X., Chu, P.K.,

Wu, S., 2017. Photo-inspired antibacterial activity and wound healing acceleration by hydrogel embedded with Ag/Ag@AgCl/ZnO nanostructures. ACS Nano 11, 9010–9021.
Mao, C., Xiang, Y., Liu, X., Cui, Z., Yang, X., Li, Z., Zhu, S., Zheng, Y., Yeung, K.W.K., Wu, S., 2018. Repeatable photodynamic therapy with triggered signaling pathways of fibroblast cell proliferation and differentiation to promote bacteria-accompanied wound healing. ACS Nano 12, 1747.
Moon, H.R., Lim, D., Suh, M.P., 2013. Fabrication of metal nanoparticles in metal–organic frameworks. Chem. Soc. Rev. 42, 1807–1824.
Qi, G., Zhang, D., Liu, F., Qiao, Z., Wang, H., 2017. An "On-site transformation" strategy for treatment of bacterial infection. Adv. Mater. 29, 1703461.
Raaymakers, C., Verbrugghe, E., Hernot, S., Hellebuyck, T., Betti, C., Peleman, C., Claeys, M., Bert, W., Caveliers, V., Ballet, S., Martel, A., Pasmans, F., Roelants, K., 2017. Antimicrobial peptides in frog poisons constitute a molecular toxin delivery system against predators. Nat. Commun. 8 1495–1495.
Ramasubbu, V., Alwin, S., Mothi, E.M., Shajan, X.S., 2017. TiO_2 aerogel–Cu-BTC metal-organic framework composites for enhanced photon absorption. Mater. Lett. 197, 236–240.
Schnaider, L., Brahmachari, S., Schmidt, N.W., Mensa, B., Shahamniv, S., Bychenko, D., Adler-Abramovich, L., Shimon, L.J.W., Kolusheva, S., DeGrado, W.F., Gazit, E., 2017. Self-assembling dipeptide antibacterial nanostructures with membrane disrupting activity. Nat. Commun. 8 1365–1365.
Sen, C.K., Khanna, S., Venojarvi, M., Trikha, P., Ellison, E.C., Hunt, T.K., Roy, S., 2002. Copper-induced vascular endothelial growth factor expression and wound healing. Am. J. Physiol. Heart Circ. Physiol. 282, H1821–H1827.
Sortino, S., 2012. Photoactivated nanomaterials for biomedical release applications. J. Mater. Chem. 22, 301–318.
Svaasand, L.O., Gomer, C.J., Morinelli, E.N., 1990. On the physical rationale of laser induced hyperthermia. Lasers Med. Sci. 5, 121–128.
Wang, S., Riedinger, A., Li, H., Fu, C., Liu, H., Li, L., Liu, T., Tan, L., Barthel, M.J., Pugliese, G., De Donato, F., Dabbusco, M.S., Meng, X., Manna, L., Meng, H., Pellegrino, T., 2015. Plasmonic copper sulfide nanocrystals exhibiting near-infrared photothermal and photodynamic therapeutic effects. ACS Nano 9, 1788–1800.
Wang, X., Li, L., Fu, Z., Cui, F., 2018. Carbon quantum dots decorated CuS NPs for effective degradation of methylene blue and antibacterial performance. J. Mol. Liq. 268, 578–586.
Wang, Z., Tang, X., Wang, X., Yang, D., Yang, C., Lou, Y., Chen, J., He, N., 2016. Near-infrared light-induced dissociation of zeolitic imidazole framework-8 (ZIF-8) with encapsulated CuS nanoparticles and their application as a therapeutic nanoplatform. Chem. Commun. 52, 12210–12213.
Wen, M., Mori, K., Kuwahara, Y., An, T., Yamashita, H., 2017. Design and architecture of metal organic frameworks for visible light enhanced hydrogen production. Appl. Catal. B 281, 555–569.
Worthington, K.S., Adamcakova-Dodd, A., Wongrakpanich, A., Mudunkotuwa, I.A., Mapuskar, K.A., Joshi, V.B., Guymon, C.A., Spitz, D.R., Grassian, V.H., Thorne, P.S., Salem, A.K., 2013. Chitosan coating of copper nanoparticles reduces in vitro toxicity and increases inflammation in the lung. Nanotechnology 24 395101–395101.
Wyszogrodzka, G., Marszalek, B., Gil, B., Dorozynski, P., 2016. Metal-organic frameworks: mechanisms of antibacterial action and potential applications. Drug Discov. Today 21, 1009–1018.
Xiang, Y., Mao, C., Liu, X., Cui, Z., Jing, D., Yang, X., Liang, Y., Li, Z., Zhu, S., Zheng, Y., Yeung, K.W.K., Zheng, D., Wang, X., Wu, S., 2019. Rapid and superior bacteria killing of carbon quantum dots/ZnO decorated injectable folic acid-conjugated pda hydrogel through dual-light triggered ros and membrane permeability. Small 15, 1900322.
Xiao, J., Zhu, Y., Huddleston, S., Li, P., Xiao, B., Farha, O.K., Ameer, G.A., 2018. Copper metal–organic framework nanoparticles stabilized with folic acid improve wound healing in diabetes. ACS Nano 12, 1023–1032.
Xiao, J., Chen, S., Yi, J., Zhang, H.F., Ameer, G.A., 2017. A cooperative copper metal–organic framework-hydrogel system improves wound healing in diabetes. Adv. Funct. Mater. 27, 1604872.
Xie, X., Mao, C., Liu, X., Zhang, Y., Cui, Z., Yang, X., Yeung, K.W.K., Pan, H., Chu, P.K., Wu, S., 2017. Synergistic bacteria-killing through photodynamic and physical actions of graphene oxide/Ag/collagen coating. ACS Appl. Mater. Interfaces 9, 26417–26428.
Xu, J., Yao, K., Xu, Z., 2019. Nanomaterials with a photothermal effect for antibacterial activities: an overview. Nanoscale 11, 8680–8691.
Xu, Z., Gao, Y., Meng, S., Yang, B., Pang, L., Wang, C., Liu, T., 2016. Mechanism and *in vivo* evaluation: photodynamic antibacterial chemotherapy of lysine-porphyrin conjugate. Front. Microbiol. 7 242–242.
Zhang, Y., Liu, X., Li, Z., Zhu, S., Yuan, X., Cui, Z., Yang, X., Chu, P.K., Wu, S., 2018. Nano Ag/ZnO-incorporated hydroxyapatite composite coatings: highly effective infection prevention and excellent osteointegration. ACS Appl. Mater. Interfaces 10, 1266–1277.
Zhu, M., Liu, X., Tan, L., Cui, Z., Liang, Y., Li, Z., Yeung, K.W.K., Wu, S., 2020. Photo-responsive chitosan/Ag/MoS_2 for rapid bacteria-killing. J. Hazard. Mater. 383, 121122.